JOURNAL OF CATALYSIS **178,** 414–428 (1998)
ARTICLE NO. CA982155

Temperature-Programmed Desorption of Oxygen from Pt Films Interfaced with Y_2O_3-Doped ZrO_2

S. G. Neophytides,[1] D. Tsiplakides, and C. G. Vayenas

Department of Chemical Engineering, University of Patras, Patras GR-26500, Greece

Received July 8, 1997; revised May 14, 1998; accepted May 21, 1998

The origin of the effect of nonfaradaic electrochemical modification of catalytic activity (NEMCA) or electrochemical promotion was investigated via temperature-programmed desorption (TPD) of oxygen from polycrystalline Pt films deposited on 8 mol% Y_2O_3-stabilized ZrO_2 (YSZ), an O^{2-} conductor, under high-vacuum conditions and temperatures of 600 to 900 K. Oxygen was adsorbed both via the gas phase and electrochemically, as O^{2-}, via electrical current application between the Pt catalyst film and a Au counter electrode. Gaseous oxygen adsorption gives a single adsorption state ($T_p \approx 720$–730 K) but electrochemical or mixed gaseous-electrochemical adsorption was found to cause significant oxygen backspillover from the YSZ solid electrolyte onto the Pt surface and the creation of two distinct oxygen adsorption states, i.e., a strongly bonded ionic state ($T_p \approx 750$–780 K) and a weakly bonded state ($T_p \approx 675$–685 K). The creation of these two states is also manifest by potentiometric work function measurements and high temperature cyclic voltammetry. These results provide a straightforward explanation of the effect of electrochemical promotion on Pt deposited on O^{2-} conducting solid electrolytes. The observed pronounced catalytic rate enhancement in electrochemical promotion studies is due to the high reactivity of the weakly bonded oxygen state, while strongly bonded ionic oxygen acts as a sacrificial promoter. The binding strength and average dipole moment of the weakly bonded oxygen state was investigated as a function of applied potential. It was found that the binding energy of adsorbed oxygen decreases linearly with increasing catalyst potential and work function in agreement with recent ab initio quantum mechanical calculations.

INTRODUCTION

The catalytic activity and selectivity of metals interfaced with solid electrolytes can be altered dramatically and reversibly by application of an electrical current or potential between the metal catalyst film and a second metal film (counter electrode) also deposited on the solid electrolyte (1–4). The increase in catalytic rate can be several, typically two to five, orders of magnitude higher than that anticipated from Faraday's law (1–4). Thus electrochemical O^{2-} supply to polycrystalline Pt catalyst films deposited on Y_2O_3-stabilized ZrO_2 (YSZ) and exposed to ethylene $-O_2$ or $CO-O_2$ mixtures causes a catalytic oxidation rate increase, Δr, which is typically 10^2–10^5 times higher than the rate, $I/2F$, of the O^{2-} supply to the catalyst. Thus each O^{2-} supplied to the catalyst causes 10^2–10^5 chemisorbed oxygen atoms to react with ethylene or CO and form CO_2 and H_2O.

During the last eight years the effect of electrochemical promotion or nonfaradaic electrochemical modification of catalytic activity (NEMCA effect) has been studied for over 50 catalytic reactions on Pt, Rh, Pd, Ag, Ni, Au, IrO_2, and RuO_2 catalyst films deposited on O^{2-}, F^-, Na^+, and H^+ conducting solid electrolytes (1–12), as well as mixed electronic-ionic conductors, such as TiO_2 (13), and aqueous alkaline solutions (14). The importance of NEMCA in catalysis (15), surface science (16), and electrochemistry (17) has been discussed and work prior to 1996 has been reviewed (3, 4). Despite the large number of different ionic conductors which have been used to induce and study electrochemical promotion most of the work in this area has utilized YSZ as the solid electrolyte.

Three parameters are commonly used to describe quantitatively the effect of electrochemical promotion:

1. The enhancement factor or faradaic efficiency, Λ, defined as

$$\Lambda = \Delta r/(I/2F), \qquad [1]$$

where Δr is the electrochemically induced change in catalytic rate (expressed in mol O/s), I is the applied current (defined positive when anions are supplied to the catalyst), and F is Faraday's constant. A reaction exhibits the NEMCA effect when $|\Lambda| > 1$. When $\Lambda > 1$ the reaction is termed electrophobic (4) and when $\Lambda < -1$ it is termed electrophilic (4); Λ values up to 3×10^5 and down to -10^4 have been measured (4).

2. The rate enhancement ratio, ρ, defined as

$$\rho = r/r_o, \qquad [2]$$

where r is the electrochemically promoted catalytic rate and

[1] Present address: Institute of Chemical Engineering and High Temperature Chemical Processes, P.O. Box 1414, Patras GR-26500, Greece.

0021-9517/98 $25.00

r_o is the open-circuit (unpromoted) catalytic rate value; ρ values up to 100 (4) or even higher (7) have been measured.

3. The promotion index, PI_i, of the promoting ion, i, defined as

$$PI_i = \frac{\Delta r/r_o}{\Delta\theta_i}, \quad [3]$$

where θ_i is the coverage of the promoting species i on the catalyst surface; PI_{Na} values up to 300 have been measured (4).

The origin of electrochemical promotion has been investigated using a variety of techniques (2, 4, 18–24). Transient kinetic measurements (4) have shown that the order of magnitude of the catalytic rate relaxation time constant, τ, upon constant current application is given by

$$\tau \approx 2FN/I, \quad [4]$$

where N is the gas-exposed catalyst film surface area expressed in moles of metal. This gave the first indication that NEMCA is due to electrochemically controlled migration (backspillover) of promoting ions from the solid electrolyte to the catalyst surface.

Work function measurements using both the Kelvin probe method (2, 22, 24) and UPS (19) have shown that the, average, work function, $e\Phi$, of the gas-exposed catalyst surface is related to its potential, V_{WR} (with respect to a reference (R) electrode), via

$$eV^o_{WR} = e\Phi_W - e\Phi_R \quad [5]$$

$$e\Delta V_{WR} = \Delta(e\Phi_W), \quad [6]$$

where V_{WR} is the catalyst-working (W) electrode potential, eV^o_{WR} stands for the open-circuit potential, and $e\Phi_W$ and $e\Phi_R$ are the average work functions of the working and reference electrodes, respectively. Equations [5] and [6] are also consistent with the spillover/backspillover ion mechanism proposed to explain the electrochemical promotion effect. The change in work function upon application of an external potential ΔV_{WR} is due to the migration of ionic species on the gas-exposed catalyst-electrode surface.

The electrochemically controlled ion backspillover mechanism has also been confirmed by XPS (18) and SERS (6, 20) for Pt electrodes deposited on YSZ and by XPS (11) and STM (21) for Pt electrodes deposited on β''-Al_2O_3. These XPS and STM studies have provided solid proof that backpillover of $O^{\delta-}$ and $Na^{\delta+}$ is a real phenomenon and can take place over very large (micrometer) distances. The mechanism of electrochemical promotion when using Na^+ conductors is thus easy to rationalize in view of the well-known promoting action of alkalis and the observation that the dipole moment of electrochemically supplied sodium is comparable to that for sodium introduced from the gas phase (4).

In the case of NEMCA, or electrochemical promotion, with O^{2-}-conducting solid electrolytes, identification of the promoting anionic oxygen species is significantly more challenging. XPS has shown that its O 1s binding energy is 528.8 eV versus 530.4 eV for normally chemisorbed oxygen which coexists on the Pt surface (18). In a recent paper (23) we have presented preliminary TPD data of oxygen on Pt films supported on YSZ. These data confirmed the electrochemically controlled oxide ion backspillover and showed that two adsorption states of oxygen are formed on polycrystalline Pt surfaces upon electrochemical O^{2-} supply versus only one adsorption state formed via gaseous O_2 adsorption. In the present work we present a detailed TPD investigation of oxygen adsorption on Pt deposited on YSZ, together with the corresponding potentiometric, and in view of Eq. [6] work function, transients, and we analyze in detail the effect of applied potential on the binding states of adsorbed oxygen. The investigation is supplemented by cyclic voltammetric data. We then analyze how the creation of the two distinct oxygen adsorption states on the Pt surface upon electrochemical O^{2-} supply can explain all the common features of electrochemical promotion of catalytic oxidations on Pt/YSZ, including the observed magnitude of the Faradaic efficiency Λ and of the rate enhancement ratio ρ.

EXPERIMENTAL

The experiments were carried out in an ultrahigh vacuum chamber (base pressure 10^{-10} Torr after baking) equipped with a quadrupole mass spectrometer (Balzers QMG 420) and a differentially pumped gas inlet system.

The polycrystalline Pt catalyst film was deposited in the form of a half-ring on the outer surface of a tubular YSZ specimen (outer diameter 19 mm, thickness 3 mm, length 30 mm) as shown on Fig. 1. The superficial surface area

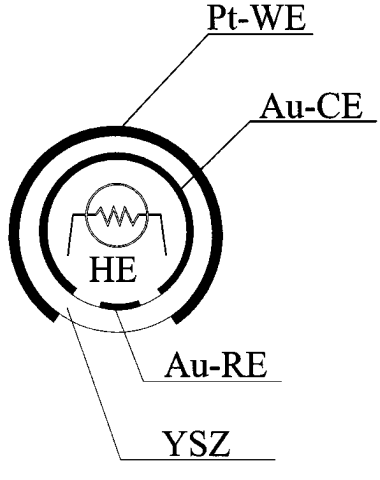

FIG. 1. Schematic cross section of the YSZ tube showing the location of the Pt film catalyst-working electrode (WE), of the Au counter (CE) and reference (RE) electrodes and of the heating element (HE).

of the Pt-film was 1.25 cm^2 and its true surface area was 80 cm^2, computed from its reactive oxygen uptake ($N_o = 2 \times 10^{-7}$ mol O) measured via isothermal titration of oxygen with CO at atmospheric total pressure, as described in detail elsewhere (4). The thus computed true surface area agrees (within 20%) with that obtained by calibrating the measured oxygen TPD peak area with that on a Pt(111) monocrystal of $2cm^2$ surface area.

The polycrystalline Pt catalyst film was deposited on the YSZ specimen as in previous NEMCA studies, i.e. by application of a thin coating of Engelhard Pt paste A-1121, followed by drying and calcination first to 450°C with heating rate 3°C/min for 1 h and then to 830°C with 2°C/min for 1 h. Scanning electron micrographs (4) and XPS survey spectra of such Pt-films have been shown previously (18). Previous XPS analysis (18) has shown either barely measurable traces of carbon or no traces at all of impurities, including C, on the Pt surface.

Gold counter and reference electrodes were deposited on the inside wall of the tubular YSZ element opposite to the Pt film (Fig. 1), by using a Au paste prepared by mixing Au powder (Aldrich powder 99.9+,32,658-5) in a slurry of polyvinyl acetate binder in ethyl acetate and by following the same calcination procedure as with the Pt catalyst (4).

A series of blank TPD experiments showed that the YSZ element and the Au electrodes do not chemisorb any measurable amounts of oxygen. Some oxygen chemisorption on Au was noted upon electrochemical O^{2-} supply to the Au counter electrode, i.e. when negative currents or potentials are applied to the present system. This electrochemical adsorption of oxygen on Au will be discussed elsewhere. However, under open-circuit conditions and also upon positive potential (and current) application the Au electrodes do not chemisorb any oxygen. Thus all the TPD spectra reported here can be safely attributed to oxygen chemisorption on the Pt film only.

Constant currents between the Pt-film and the Au counter electrode (galvanostatic operation) or constant potentials V_{WR} between the Pt film and the Au reference electrode were applied using an AMEL 553 galvanostat–potentiostat. The same potentiostat, in conjunction with an AMEL 567 function generator, was used for the cyclic voltammetric experiments. Pt wires were used to connect the Pt film and Au auxiliary electrodes with the galvanostat–potentiostat.

The work function, $e\Phi$, of the polycrystalline Pt film could also be monitored continuously by measuring its ohmic drop-free potential V_{WR} with respect to the reference Au electrode and utilizing Eq. [6].

The specimen was heated radiatively using an Osram Xenon lamp located inside the tubular YSZ specimen (Fig. 1). A type-K thermocouple attached to the Pt film was used to measure the temperature. The temperature could be varied linearly at a heating rate as high as 2 K/s, using a Eurotherm programmable temperature controller.

Three modes of oxygen adsorption on the Pt catalyst surface were used for the thermal desorption experiments:

1. Gaseous oxygen adsorption by exposure to $P_{O_2} = 4 \times 10^{-6}$ Torr for various periods of time, denoted t_{O_2}.
2. Electrochemical oxygen adsorption, by application of positive currents I between the Pt catalyst and the Au counter electrode for various periods of time, denoted t_I. In this case oxygen is supplied to the Pt film at a rate $I/2F$ (4) and is depleted from the YSZ solid electrolyte in the vicinity of the counter electrode at the same rate.
3. Mixed gaseous and electrochemical adsorption. In this case oxygen is first adsorbed from the gas phase for a time t_{O_2}, followed by electrochemical supply of oxygen for a time t_I.

Oxygen adsorption was carried out at temperatures 623–673 K, followed by cooling the sample to 573 K and then increasing the temperature linearly at a rate β (K/s).

In order to determine the oxygen desorption activation energy, E_d, and its dependence on catalyst potential a series of low coverage TPD experiments was carried out. The exact experimental procedure was the following: A constant positive current I was applied for a time t_I to supply oxygen to the catalyst at a rate $I/2F$ and to establish a small initial coverage of oxygen θ_o on the Pt catalyst surface. This initial oxygen coverage θ_o was kept as constant as possible within experimental error (~10%) in order to facilitate the TPD data analysis. In eight different sets of experiments this current application was performed at eight different temperatures between 583 and 723 K. Owing to the increasing effect of T on the exchange current I_0 of the Pt–YSZ interface (4), the induced catalyst potential V^*_{WR} at the end of the time of current application t_I varied between 0.6 and 0.06 V for the two extreme temperatures of current application of 583 and 723 K, respectively.

At the end of t_I the current was stopped, and the sample was rapidly cooled to 520 K without any significant change in the open circuit potential V^*_{WR}. The sample temperature was then increased at a heating rate β (K/s) to obtain the TPD spectra.

In each of the eight sets of experiments (i.e., starting the TPD from the same temperature (520 K) and the same initial oxygen coverage but different catalyst potential V^*_{WR} values), four to six different heating rates β were used ranging from 0.4 to 2 K/s. We thus obtained 48 different peak desorption T_p values ranging from 638 to 795 K and corresponding to different pairs of V^*_{WR} and β. These data were used to extract the activation energy of oxygen desorption E_d via the standard Redhead analysis as generalized by Falconer and Madix (25). Note that in this analysis, which is valid for any positive order desorption kinetics

(25), no assumption has to be made about a specific form of the desorption kinetic expression. The above experimental procedure, regarding t_I and V^*_{WR}, was followed during all electrochemical and mixed adsorption experiments, including those with high initial oxygen coverage. Thus V^*_{WR} always refers to the catalyst potential value at the end of current application and thus also at the start of the TPD spectrum.

RESULTS AND DISCUSSION

1. *Gaseous Adsorption*

Figure 2a shows typical oxygen thermal desorption spectra after catalyst exposure to oxygen partial pressure, $P_{O_2} = 4 \times 10^{-6}$ Torr at 673 K for various oxygen exposure times, t_{O_2}. The exposure is expressed in kilolangmuirs, kL, where 1 kL $= 10^{-3}$ Torr · s. There is a single oxygen desorption

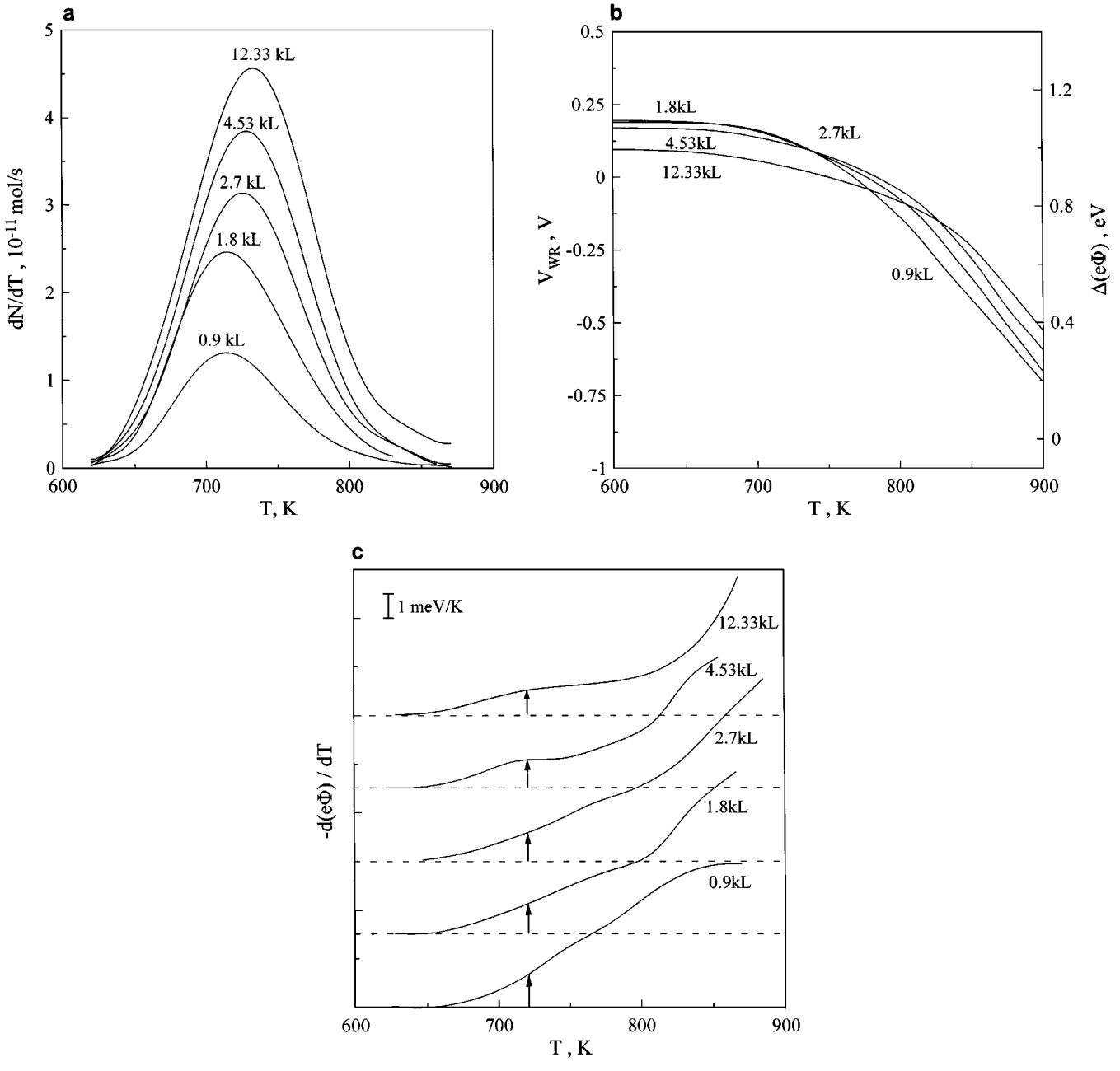

FIG. 2. (a) Thermal desorption spectra after gaseous oxygen dosing at 673 K and an O_2 pressure of 4×10^{-6} Torr for various exposure times. Oxygen exposure is expressed in kilolangmuirs (1 kL $= 10^{-3}$ Torr · s). Desorption was performed with linear heating rate, $\beta = 1$ K/s. (b) Variation of film potential and work function change vs Au reference electrode corresponding to the TPD spectra of (a). (c) $d(e\Phi)/dT$ curves during the TPD spectra of (a). Arrows connect each curve with zero baseline.

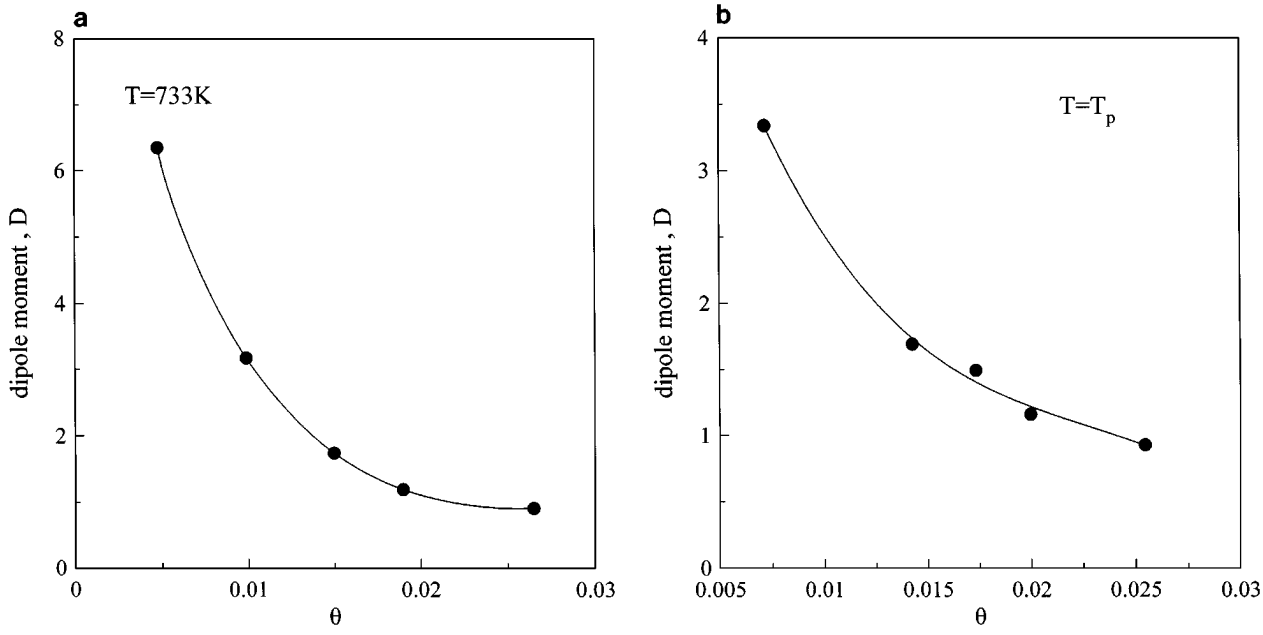

FIG. 3. (a) Variation of oxygen dipole moment with coverage at 733 K obtained from Figs. 2a and 2c; gaseous adsorption. (b) Variation of oxygen dipole moment with coverage at peak desorption temperature obtained from Figs. 2a and 2c; gaseous adsorption.

peak with peak temperature at $T_p = 718 \pm 5$ K. Increasing oxygen coverage leads to a small (∼10 K) increase in T_p, indicating some weak overall attractive interactions between chemisorbed oxygen atoms. Similar results have been reported from studies on Pt single crystals and polycrystalline samples (26, 27). The asymmetric shape of the peaks can be explained by the coexistence of a second peak, as suggested from previous XPS investigations (28).

Figure 2b shows the transient behavior of catalyst potential V_{WR}, and thus work function change, $\Delta(e\Phi)$, corresponding to the TPD spectra of Fig. 2a. Increasing oxygen exposure and, consequently, oxygen coverage increases the work function by up to 1 eV, in good agreement with literature (28, 29). By differentiation of the V_{WR} versus T curves one obtains Fig. 2c. As shown in this figure for high oxygen exposures the $-d(e\Phi)/dT$ curves exhibit a shallow maximum near the peak desorption temperature of 718 K (Fig. 2a). This maximum disappears at lower exposures.

Figures 2a and 2c can be used to obtain an estimate of the average dipole moment, P_o, of oxygen adsorbed on Pt via the differential form of the Helmholtz equation,

$$\frac{d(e\Phi)}{dt} = -e \cdot \frac{P_o}{\varepsilon_o} \cdot \frac{dN}{dt} \cdot \frac{N_{AV}}{A}, \qquad [7]$$

where $e = 1.6 \times 10^{-19}$ C, $\varepsilon_o = 8.85 \times 10^{-12}$ C^2/(J · m), N_{AV} is the Avogadro number, A is the surface area, and dN/dt is the desorption rate. To this end dN/dt is computed from the thermal desorption spectra (Fig. 2a) and $d(e\Phi)/dt$ from Fig. 2c. The thus computed oxygen dipole moment is plotted in Fig. 3 versus oxygen coverage at constant temperature $T = 733$ K (Fig. 3a) and at the peak temperature (Fig. 3b). The oxygen coverage is computed using the TPD spectra (Fig. 2a) and the atmospheric pressure maximum reactive oxygen uptake ($N_O = 2 \times 10^{-7}$ mol O). In both cases, the dipole moment decreases with increasing oxygen coverage, reaching a constant value of about 1 Debye, in accordance with literature (29, 30).

Figure 4a shows the effect of oxygen exposure time (at $P_{O_2} = 4 \times 10^{-6}$ Torr and $T = 673$ K) on oxygen coverage. The maximum oxygen coverage obtained via gaseous adsorption is small, typically less than 0.03. The sticking coefficient for gas phase adsorption, S, is defined as the ratio of the adsorbed oxygen molecules (estimated from integration of the thermal desorption spectra) over the total oxygen molecules that collide with the surface, i.e. $(P_{O_2}/(2\pi MRT_g)^{1/2}) \cdot A \cdot t_{O_2}$, where P_{O_2} is the oxygen partial pressure in Torr, M is the molecular weight of O_2, R is the gas constant, T_g is the gas temperature, A is the total surface area of the catalyst film, and t_{O_2} is the oxygen exposure time. For gas phase adsorption at a surface temperature of 673 K the integrated sticking coefficient is of the order of 10^{-5} (Fig. 4b). There are two reasons for the observed low value of the sticking coefficient and the concomitantly low oxygen coverage at saturation (Fig. 4a). First is the high adsorption temperature (673 K). Most previous sticking coefficient measurements have been performed on Pt surfaces at room temperature or below (27, 31–33). It is well established that atomic oxygen chemisorption proceeds via a molecularly adsorbed precursor state the coverage of which

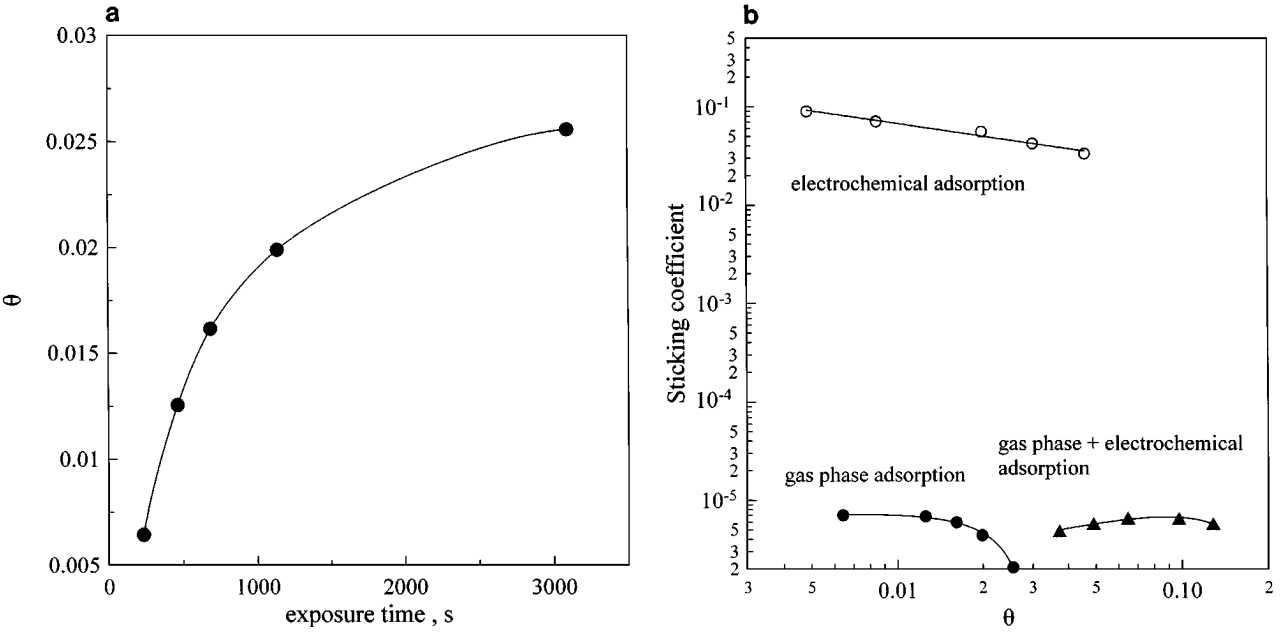

FIG. 4. (a) Effect of exposure time at $P_{O_2} = 4 \times 10^{-6}$ Torr on oxygen coverage for gaseous oxygen adsorption at 673 K. (b) Integrated sticking coefficient as a function of coverage for the three modes of oxygen adsorption at 673 K: (●) gaseous oxygen adsorption at an O_2 pressure of 4×10^{-6} Torr; (○) electrochemical O^{2-} supply, $I = +15\ \mu A$; (▲) gaseous oxygen adsorption at an O_2 pressure of 4×10^{-6} Torr for 1800 s followed by electrochemical O^{2-} supply, $I = +15\ \mu A$.

decreases exponentially with increasing temperature (27, 34–36). Consequently the sticking coefficient also decreases very strongly with increasing temperature. The second reason must be the occurrence of the "clean-off" reactions due primarily to the H_2, and trace amounts of CO, of the vacuum system background. These "clean-off" reactions become automatically quite important at the elevated temperatures of the present investigation, due to the high catalytic activity of the Pt surface.

2. *Electrochemical Adsorption*

Figure 5a shows typical thermal desorption spectra obtained after electrochemical O^{2-} supply to the Pt-catalyst film through the solid electrolyte at 673 K for various periods of current application, t_I. For small t_I only one peak is present at about 693 ± 10 K, which is almost 25 K lower than the peak obtained from gas phase adsorption. The situation changes dramatically after prolonged current application as a second high temperature peak develops between 723 and 773 K, along with the low temperature peak. The low temperature peak corresponds to more weakly bounded atomic oxygen, which, as shown below, is the same type of oxygen which forms via gas-phase adsorption and has displaced to more weakly bonded sites. The high temperature peak, which develops only after prolonged current application ($\sim 2FN_o/I = 2570$ s, for the experiment of Fig. 5a) and, consequently at higher oxygen coverage, is attributed to the strongly bonded "ionic" or "backspillover" oxygen (4). It should be emphasized that this peak does not form via gas-phase adsorption. Exactly the same behavior has been observed in the *in situ* XPS investigation of the system Pt/YSZ (18). In brief, the XPS spectra showed two oxygen O 1s peaks, one at 530.4 eV (normally adsorbed atomic oxygen) and one at 528.8 eV (ionic oxygen species), the latter state developing only after prolonged current application ($\sim (2FN_o/I) \cdot S$) which is the time required to form a monolayer of oxygen on a surface with N_o sites when it is supplied at a rate $I/2F$ and the sticking coefficient is S . As shown in Fig. 4b and analyzed below, the sticking coefficient, S, for electrochemical adsorption is of the order of 0.1 at 673 K. Electrochemically supplied oxygen which does not stick on the surface desorbs in the gas phase.

The transient behavior of the Pt-film potential, V_{WR}, and work function change, $\Delta(e\Phi)$, versus the Au reference electrode, corresponding to the TPD spectra of Fig. 5a, is presented on Fig. 5b. The situation is very different, compared to the thermal desorption following gas-phase adsorption. The film potential versus temperature curves present one (for short current application) or two (for prolonged current application) inflection points. It is noteworthy that the appearance of the ionic oxygen on the Pt surface is accompanied by a significant (up to 0.6 eV) increase in its work function, relative to that obtained from gaseous adsorption. This further corroborates the ionic nature of the high temperature oxygen species. The existence of inflection points becomes very clear when we differentiate these curves (Fig. 5c). As expected, the inflection points on V_{WR}

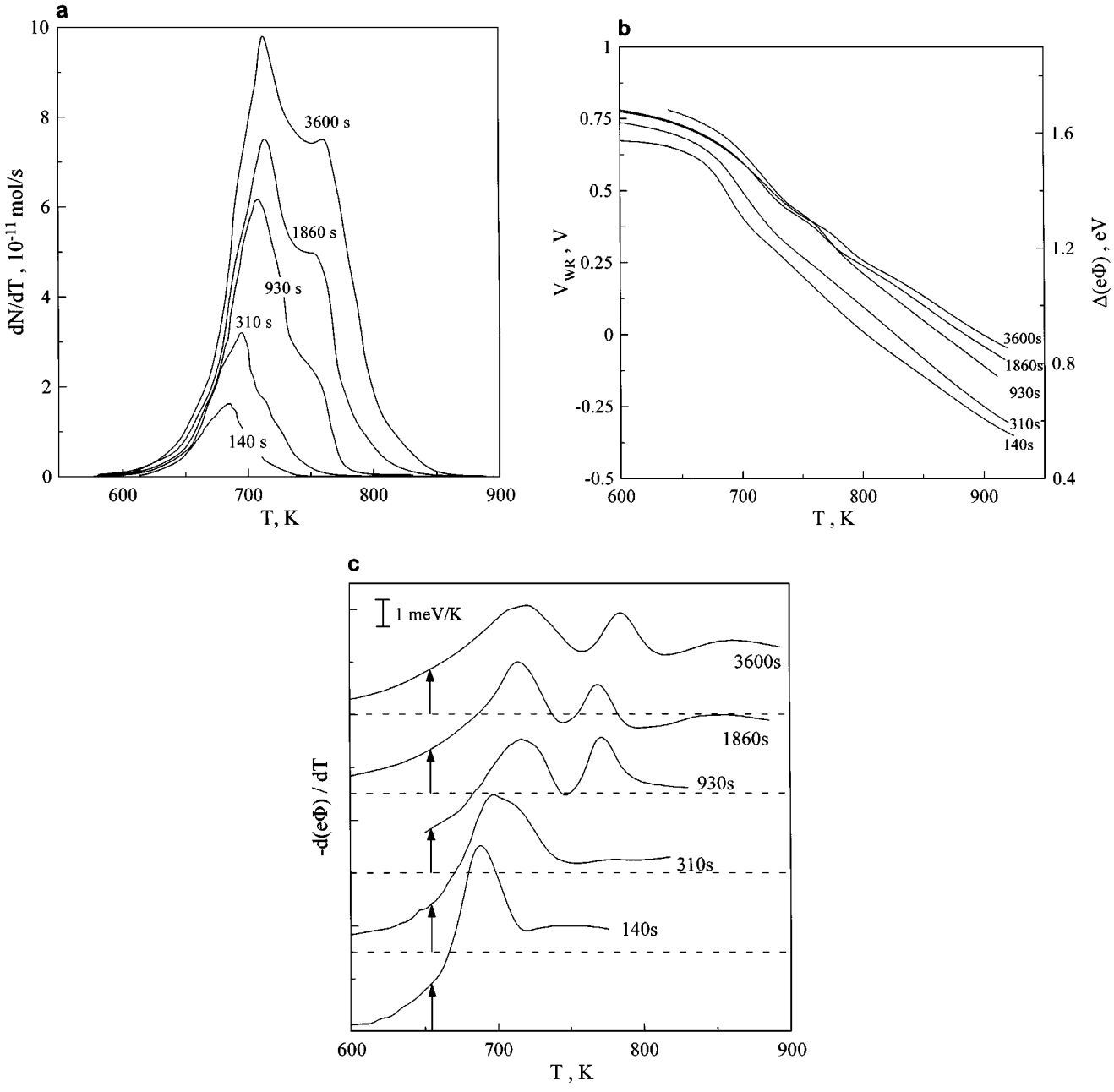

FIG. 5. (a) Thermal desorption spectra after electrochemical O^{2-} supply at 673 K. The different curves correspond to various times of current application; $I = +15\ \mu A$. Desorption was performed with linear heating rate, $\beta = 1$ K/s; $2FN_O/I = 2570$ s. (b) Variation of film potential and work function change corresponding to the TPD spectra of Fig. 5a. (c) $d(e\Phi)/dT$ curves during the TPD spectra of Fig. 5a.

versus T curves give rise to local maxima in the $-d(e\Phi)/dT$ versus T curves. The latter parallel closely the corresponding thermal desorption spectra (Fig. 5a), as the local maxima are at about the same temperature as the desorption peaks.

Following the same procedure as in gaseous adsorption, the dipole moment during desorption can be extracted. The dipole moment values at the first peak temperature are plotted against total oxygen coverage at this temperature in Fig. 6. The dipole moment is very high at low coverage and reaches an asymptotic constant, value of 2 Debye at $\theta \approx 0.05$, which is twice the value of the dipole moment of oxygen after gas-phase adsorption. This is another indication for the weakening of the bond of chemisorbed atomic oxygen with Pt, induced by the presence of ionic oxygen species. As the bond strength is reduced, the bond length and dipole moment increase.

The sticking coefficient in electrochemical adsorption can be defined as the ratio of adsorbed oxygen molecules,

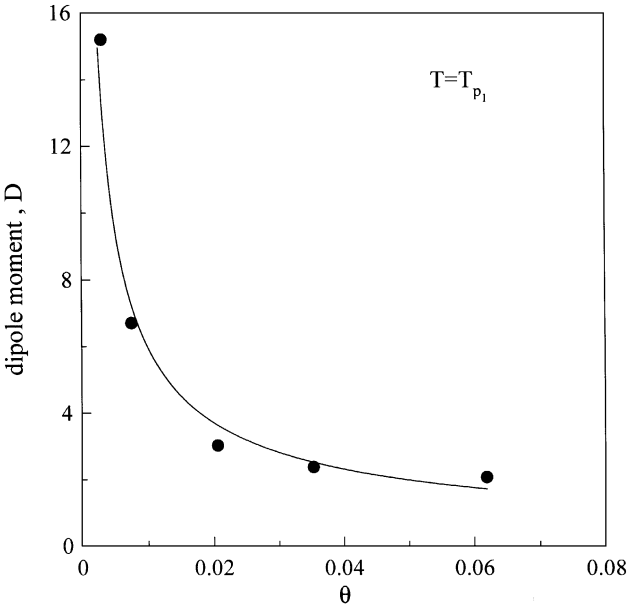

FIG. 6. Oxygen dipole moment at first peak temperature for the desorption spectra of Fig. 5a, showing its dependence on the corresponding oxygen coverage.

calculated from integration of the TPD spectra, over the supplied oxygen atoms through the solid electrolyte ($=(I/2F)\cdot t_I$ for constant positive current application). Figure 4b shows the effect of total oxygen coverage on the sticking coefficient. The sticking coefficient on electrochemical adsorption decreases with coverage ($S\sim\theta^{-0.4}$) and its value is about 10^4 times larger than in the case of gaseous adsorption. The relatively high values of S is a general observation when oxygen is supplied electrochemically (37).

3. *Mixed Gaseous and Electrochemical Adsorption*

Figure 7a shows typical oxygen thermal desorption spectra obtained after gaseous oxygen adsorption at $P_{O_2}=4\times10^{-6}$ Torr for 1800 s (7.2 kL) at 673 K followed by electrochemical supply of O^{2-}, at a rate $I/2F$, at 673 K for various current application times, t_I. After prolonged current application at least two, and possibly three, oxygen peaks are developed. Figure 7a provides a clear explanation of the NEMCA effect when using O^{2-} conductors, in excellent agreement with the XPS (18) and SERS (20) investigations and with the previously developed theory to interpret kinetic NEMCA studies (4): Electrochemically supplied O^{2-} produces strongly bonded "ionic" or "backspillover" oxygen ($T_p=723$ to 773 K) over a time period of the order of $2FN_O/I$ (=2570 s) with a concomitant pronounced lowering (up to 50 K, i.e. from 743 to 693 K) of the desorption temperature of the more weakly bound atomic oxygen. This pronounced weakening in the Pt=O bond causes the observed dramatic catalytic rate enhancement in NEMCA studies, while the strongly bonded oxygen state acts as a sacrificial promoter. There are two points that should be noted. First, these oxygen adsorption states do not form via gas-phase adsorption. Second, the presence of gas-phase oxygen is necessary for obtaining a nonfaradaic rate enhancement. Even though the weakly bonded state forms also when there is only electrochemical O^{2-} supply (Fig. 5a), in this case simple mass balance considerations dictate that any catalytic oxidation rate has to be faradaic ($\Lambda\leq1$), since all the oxygen is supplied electrochemically.

Figure 7b shows the transient behavior of film potential, V_{WR}, and work function change, $\Delta(e\Phi)$, during thermal desorption. Following the same procedure as in the other two modes of adsorption, we obtain the $-d(e\Phi)/dT$ versus T curves (Fig. 7c) and the dipole moment at the first peak temperature (Fig. 8). The shape of these figures is similar to the curves obtained after gaseous and electrochemical adsorption. As in the cases of gaseous adsorption and electrochemical adsorption the dipole moment decreases with coverage and reaches asymptotically a constant value. This value (~1 D) is very close to that obtained during electrochemical adsorption.

By combination of the definition of the sticking coefficient upon gas-phase and electrochemical adsorption, one can compute S also under conditions of mixed adsorption. The variation of S with coverage is shown on Fig. 4b. In this case the sticking coefficient remains almost constant over the whole range of oxygen coverage examined.

4. *Thermal Desorption Following Isothermal Desorption*

Figure 9 shows the effect of isothermal oxygen desorption at 673 K on the thermal desorption spectrum of electrochemically supplied oxygen. In these experiments oxygen is supplied electrochemically, at a constant rate $I/2F$ for 1800 s at 673 K, followed by isothermal desorption at 673 K for various desorption times, t_d, with subsequent rapid cooling to 573 K and starting the TPD experiment.

As expected, the low temperature peak (atomic oxygen) disappears much faster than the high temperature peak (ionic oxygen). After sufficient (>160 s) desorption time, only the high temperature peak remains which corresponds to ionic backspillover oxygen. This isolation of the ionic spillover oxygen species via isothermal desorption is very similar with the procedure used to isolate the same species in UHV and obtain its XPS spectrum (18), which confirmed the strong anionic nature of the backspillover oxygen species due to its very low O 1s binding energy (18).

By deconvolution of the desorption spectra following isothermal desorption (Fig. 9), we can compute the peak desorption rate of the two oxygen species, i.e. the peak desorption rate from the low and the high temperature oxygen states. By plotting the logarithm of the peak desorption rates of each species against the desorption time, one can obtain an estimate of the desorption constant, k_d, from the slope of each line, (Fig. 10) (assuming first-order

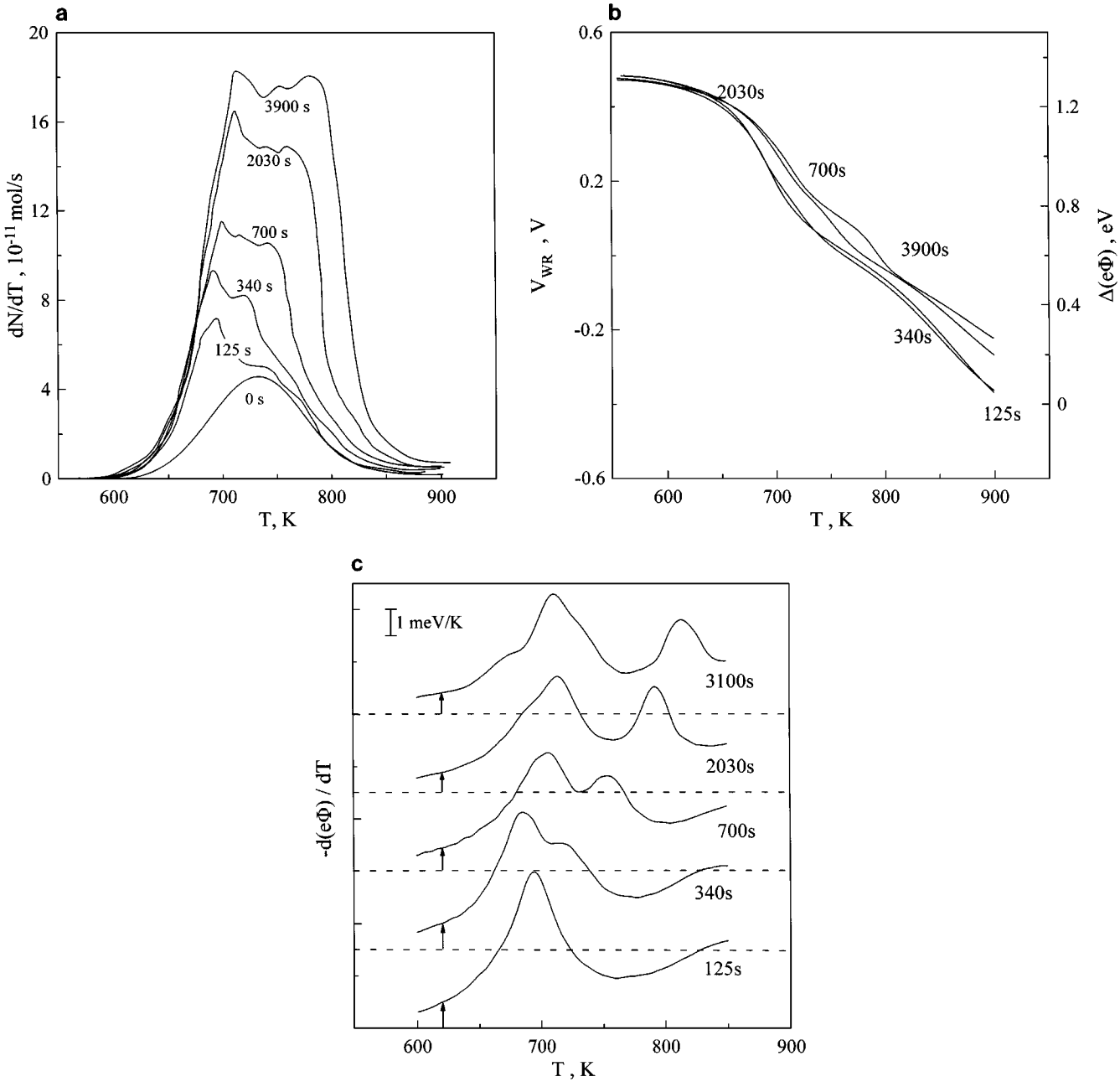

FIG. 7. (a) Thermal desorption spectra after gaseous oxygen adsorption at 673 K and an O_2 pressure of 4×10^{-6} Torr for 1800 s (7.2 kL) followed by electrochemical O^{2-} supply ($I = +15\ \mu A$) for various time periods. Desorption was performed with linear heating rate, $\beta = 1$ K/s; $2FN_O/I = 2570$ s. (b) Variation of film potential and work function change corresponding to the TPD spectra of Fig. 7a. (c) $d(e\Phi)/dT$ curves during the TPD spectra of Fig. 7a.

desorption). We thus can estimate the ratio of the two desorption constants, termed Λ_d. Since the low temperature oxygen state corresponds to the normal adsorbed oxygen and the high temperature state corresponds to the ionic oxygen, the ratio Λ_d provides a measure of the relative propensity of the two species for desorption. Thus, the weakly bonded atomic oxygen is about seven times more active for desorption ($\Lambda_d = 7$) than the ionic backspillover oxygen species.

The relative propensity of the two oxygen species for desorption provides also a relative qualitative measure of their relative oxidative propensity, e.g. during C_2H_4 or CO oxidation, under conditions where cleavage of the metal–oxygen bond is rate limiting. The ratio of the reaction rate of the two oxygen states with coadsorbed oxidizable species (e.g., C_2H_4 or CO) can be identified as the faradaic efficiency, Λ, during the corresponding oxidation reaction. This is assuming that electrochemically supplied oxygen (at a rate $I/2F$

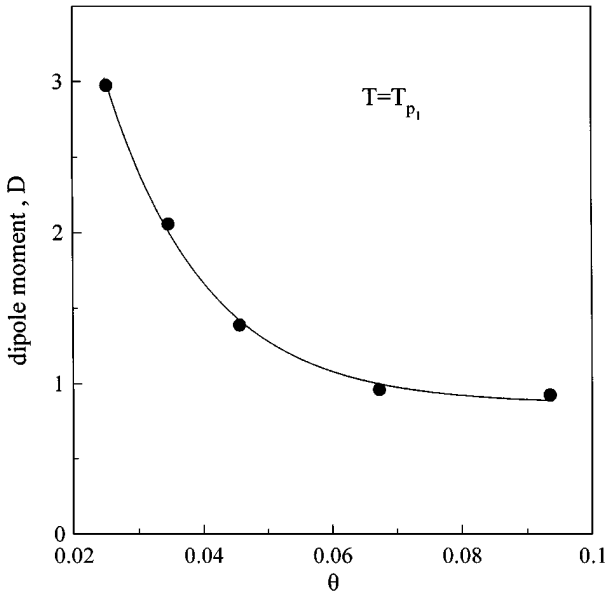

FIG. 8. Variation of the oxygen dipole moment with coverage at the first peak desorption temperature obtained from Figs. 7a and 7c; electrochemical adsorption.

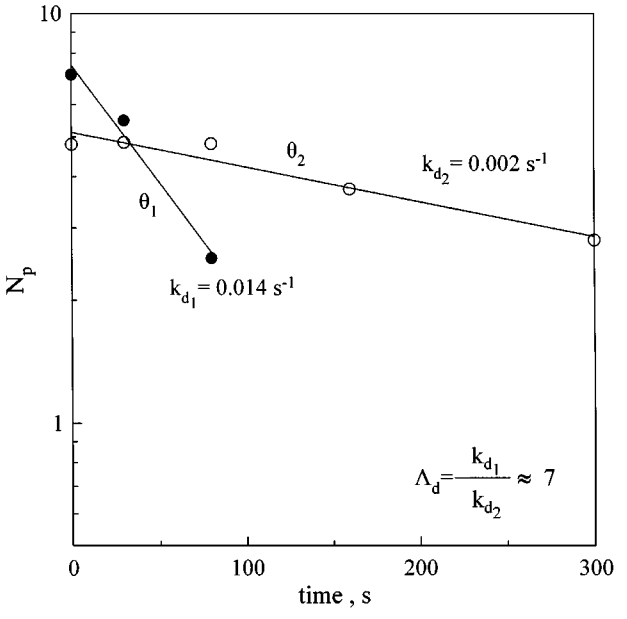

FIG. 10. Effect of isothermal desorption time on the peak desorption rate of the high (○) and low (●) temperature peaks. The peak desorption rates were calculated after deconvolution of the TPD spectra following isothermal desorption at 673 K.

during a steady-state NEMCA experiment) populates primarily the strongly bonded ionic state (Fig. 7a) and, also, assuming that the total measured catalytic rate r (which practically coincides with Δr in NEMCA experiments with $\rho = r/r_o \gg 1$) is due primarily to the reaction of the weakly bonded oxygen (Fig. 7a). Thus, since $\Lambda = \Delta r/(I/2F)$, it follows that, indeed, under these assumptions Λ can be identified as the ratio of reaction of the two oxygen species with the coadsorbed oxidizable reactant (e.g., C_2H_4 or CO). Figure 11 compares the measured Λ_d value with Λ values measured during C_2H_4 oxidation on various metal catalysts supported on YSZ (4). Two observations can be made.

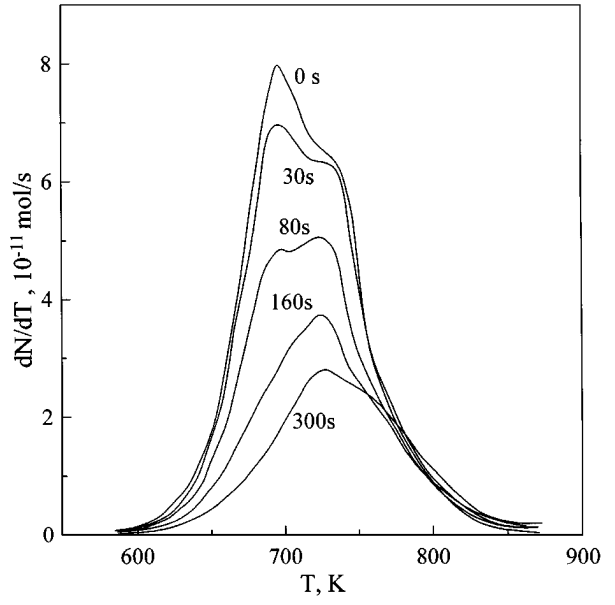

FIG. 9. Oxygen thermal desorption spectra after electrochemical O^{2-} supply at 673 K ($I = +12\ \mu A$ for 1800 s), followed by isothermal desorption at the same temperature at various times as indicated on each curve.

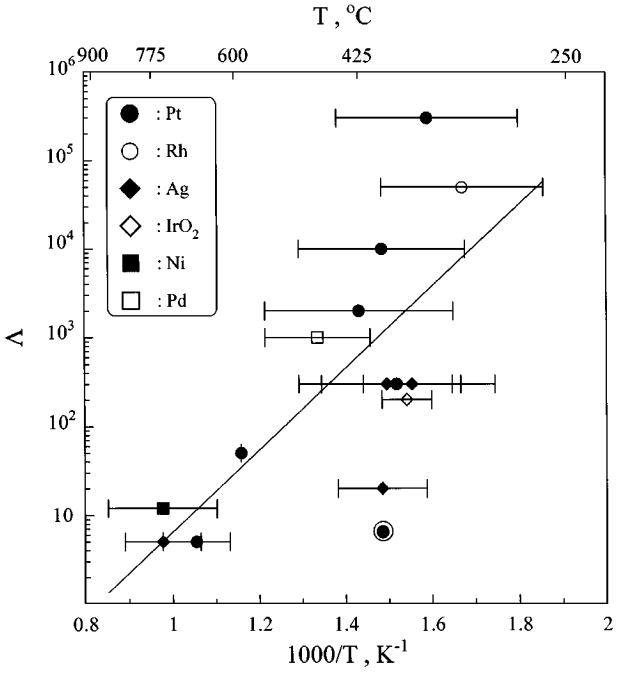

FIG. 11. Effect of temperature on the faradaic efficiency, Λ, values measured in electrochemical promotion (NEMCA) studies of catalytic oxidations (based on Table 3 of Ref. (4)) and comparison with Λ_d defined in text (◉).

First, the measured Λ_d value for oxygen desorption is significantly lower than Λ values measured during C_2H_4 oxidation on Pt. This may be due to the much higher value of the activation energy for oxygen desorption (in the range of 50 kcal/mol as discussed below), compared with the measured values of the activation energy of ethylene oxidation on Pt (in the range 15–20 kcal/mol). Second, it should be noticed in Fig. 11 that Λ approaches unity as the temperature is increased. This can be rationalized directly in view of the TPD spectra (e.g., Figs. 5a, 7a) which show that above 800 K the coverage of both oxygen species, including the strongly bonded ionic oxygen species, practically vanish. Consequently the state of adsorbed oxygen cannot be further influenced by electrochemically supplied oxygen and the catalytic rate increase Δr is just equal to the electrochemical supply of oxygen; i.e., $\Lambda = \Delta r/(I/2F)$ becomes unity.

5. *Thermal Desorption at Low Coverage*

In order to investigate the effect of catalyst potential on the binding strength of atomically adsorbed oxygen, a series of low coverage thermal desorption experiments was carried out at various imposed catalyst potentials as described in the experimental section. In these experiments oxygen was supplied electrochemically and the current application time was chosen so that the resulting initial oxygen coverage was practically constant for all the different applied potentials. Under these low coverage conditions the ionic oxygen peak does not appear. This set of experiments was carried out at various heating rates, β, and the modified Redhead equation of Falconer and Madix (25) was used to extract the activation energy of oxygen desorption, E_d,

$$\ln\left(\beta/T_p^2\right) = \ln\left(R\cdot\nu\cdot\theta_o^{n-1}/E_d\right) - E_d/RT_p, \qquad [8]$$

where ν is the preexponential factor, n is the desorption order, and θ_o is the initial coverage. As shown on Fig. 12, a plot of $\ln(\beta/T_p^2)$ versus $1/T_p$ gives a straight line, in good agreement with Eq. [8], and the slope equals $-E_d/R$. An alternative method for the determination of E_d is the low coverage method (38). Starting from the basic desorption rate equation,

$$\frac{dN}{dT} = (\nu/\beta)\cdot\theta^n \exp\left(-\frac{E_d}{RT}\right), \qquad [9]$$

by differentiation we obtain

$$\frac{d\ln(dN/dT)}{d(1/T)} = -\frac{E_d}{R} + \frac{dl(\nu/\beta)}{d(1/T)} + \frac{d\ln\theta}{d(1/T)}. \qquad [10]$$

Assuming that ν and θ do not change with temperature, then we can neglect the two last terms of the above equation and, hence, the slope of $\ln(dN/dT)$ versus $1/T$ is equal to $-E_d/R$. This is valid only for the left "tail" of the desorption spectra, that is, low desorption temperatures. The low coverage method is applied to the thermal desorption spectra after electrochemical O^{2-} supply at various temperatures and polarization resulting in high oxygen coverage (Fig. 13). The estimated E_d values from both the above methods are plotted in Fig. 14a as a function of catalyst potential. Interestingly, the data from both methods fall on a straight line with slope -1, with E_d decreasing from 2.14 eV to 1.42 eV as V_{WR} is increased by 0.7 V. This confirms that the catalyst potential and work function have a pronounced effect on the binding strength of atomic oxygen. This linear decrease of the activation energy for desorption and, thus, the binding energy with increasing catalyst potential and work function is in excellent qualitative agreement with recent *ab initio* quantum-mechanical calculations of Pacchioni *et al.* (39) who found a linear decrease with slope -0.5.

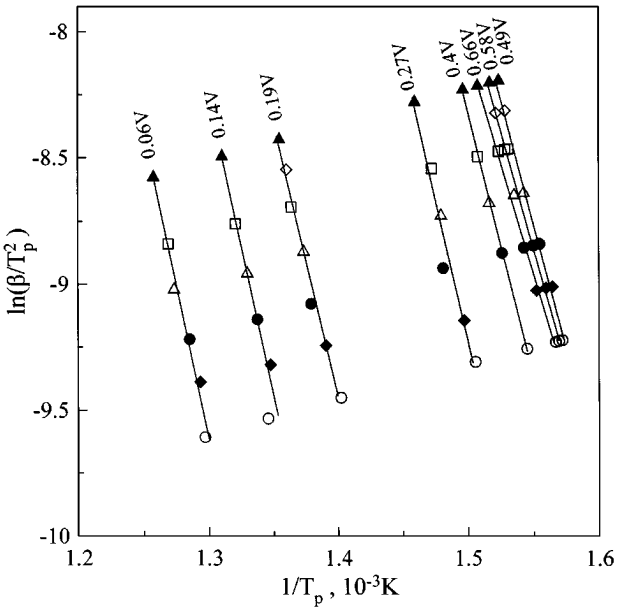

FIG. 12. $\mathrm{Log}(\beta/T_p^2)$ as a function of $1/T_p$ for various catalyst film potentials versus Au reference electrode. The slope of each curve is equal to E_d/R, according to the modified Redhead analysis of Madix and Falconer (Ref. (25)).

From the same set of data used for the determination of E_d from Eq. [8], it is possible to determine the preexponential factor of desorption. Starting from the basic desorption rate equation and by differentiation with respect to coverage, we obtain at the peak temperature (38):

$$\beta\cdot\left(\frac{E_d}{RT_p^2}\right)\cdot\exp\left(\frac{E_d}{RT_p}\right) = \nu + \theta\cdot\frac{dN}{d\theta} - N\cdot\frac{\theta}{RT_p}\cdot\frac{dE_d}{d\theta}. \qquad [11]$$

Under certain conditions (38) one can neglect that last two terms of the right side of the equation and in this way compute the preexponential factor, ν, simply as the left part of the equation. The main assumption made is that the

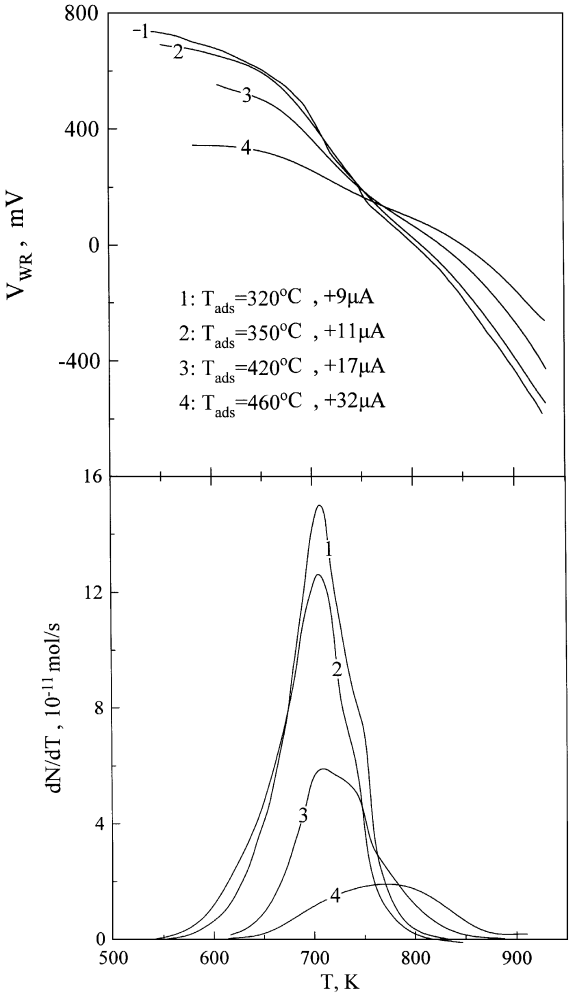

FIG. 13. Thermal desorption spectra (bottom) and corresponding catalyst potential variation (top) after electrochemical O^{2-} supply at various temperatures and polarizations.

desorption follows a first-order rate, which is the case as shown later. The thus computed values of ν are plotted against catalyst film potential (Fig. 14b) and against desorption activation energy (Fig. 14c). In both cases, the preexponential factor exhibits a sharp maximum, which may be indicative of adsorption on different sites, depending on the film potential. The low E_d data of Fig. 14c demonstrate the well-known compensation effect (40); i.e., the preexponential factor increases linearly with the desorption activation energy and the two are related with a simple equation,

$$\ln \nu = E_d/RT_\Theta + c, \qquad [12]$$

where c is a constant and T_Θ is an isokinetic temperature. The isokinetic temperature is calculated from the slope of Fig. 14c to be about 663 K. From the data of the activation energy and the preexponential factor (Fig. 14b) we can compute the desorption rate constant, k_d, at every temperature for each catalyst potential. Then we plot the ratio, ρ_d, of k_d for various potentials over k_d evaluated at the lowest applied catalyst potential $V^*_{WR} = 0.06\ V$ against $1/T$ (Fig. 14d, straight lines). In view of Eq. [12] all lines corresponding to high potentials meet at a single point, the isokinetic point of desorption, at $T = 663$ K, where under all catalyst potentials the desorption rate is the same. At low potentials there is no isokinetic point and ρ_d increases monotonically with potential. This ratio, ρ_d, provides a measure of the increase in the propensity of adsorbed oxygen for desorption due to the applied potential. In a qualitative sense it also provides a measure of its increased reactivity for oxidation reactions under conditions where cleavage of metal–oxygen bond is rate limiting. Previous electrochemical promotion studies have shown ρ values of up to 100 for C_2H_4 oxidation on Pt. Figure 14d predicts even higher ρ_d values for oxygen desorption (straight lines). Figure 14d also shows experimental ρ_d values (filled circles) obtained from the high coverage desorption data of Fig. 13. In this case k_d and, thus, ρ_d are evaluated from $k_d = (dN/dt)/\theta$, where the θ value corresponding to each temperature, potential, and corresponding (dN/dt) value is computed by integration of the TPD spectrum to the right of the corresponding temperature. It can be seen that the measured ρ_d values are up to 700 but are in general lower than those predicted from the low coverage data (straight lines). They increase with increasing potential and, as the predicted ρ_d values, decrease with increasing temperature.

In order to support the assumption of near first-order desorption made to compute preexponential factors we use the high coverage data of Fig. 13. Starting again from the basic desorption rate equation (Eq. [9]), by taking the logarithm we obtain (41)

$$\ln(dN/dt) = \ln \nu + n \ln \theta - E_d/RT. \qquad [13]$$

Consequently the plot of $\ln(dN/dt)$ versus $\ln \theta$ for constant temperature is a straight line with slope equal to n, if the desorption activation energy is weakly dependent on coverage. As shown in Fig. 15 this is indeed the case and the slopes of these lines are equal to 0.8–0.95; i.e. close to first-order desorption.

6. *Cyclic Voltammetry*

Figures 16a and 16b show results of the cyclic voltammetric investigation in the absence of gaseous oxygen and with $P_{O_2} = 4 \times 10^{-6}$ Torr, respectively, obtained by varying the holding time at $V_{WR} = 0.8\ V$ at 673 K. The cyclic voltammetric peaks in Figs. 16a and 16b are due to the charge transfer reaction:

$$O^{2-} \leftrightarrows O(a) + 2e^-, \qquad [14]$$

where O^{2-} is oxygen in the YSZ solid electrolyte and O(a) is oxygen adsorbed on the Pt surface (42). When reaction [14] proceeds to the right (anodic operation) the current is

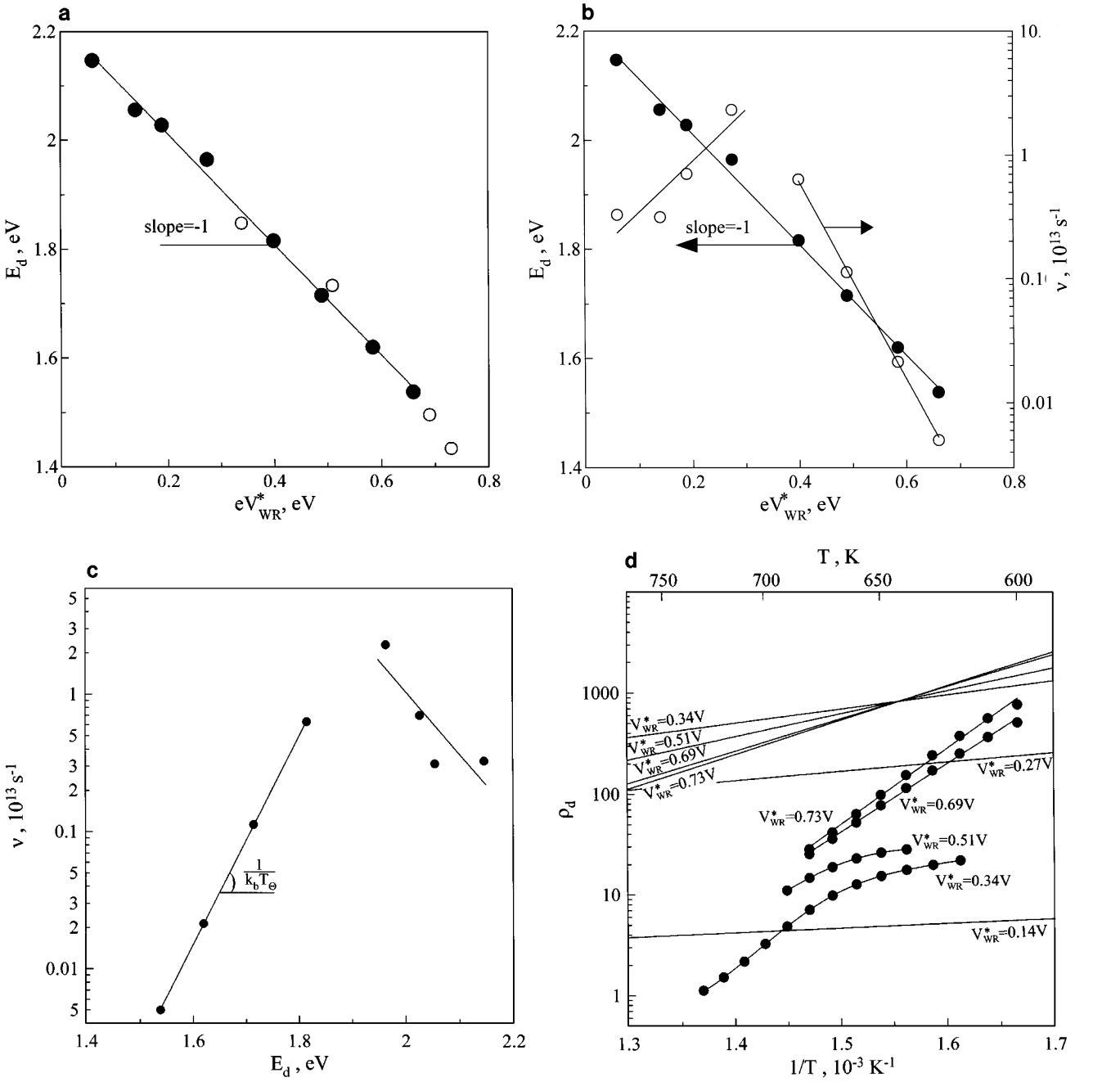

FIG. 14. (a) Effect of catalyst potential on the desorption activation energy calculated from the modified Redhead analysis (●) and from the initial slope of the TPD spectra of Fig. 13 (○). (b) Effect of catalyst potential on desorption activation energy (●) and on first order preexponential factor (○). (c) Dependence of the preexponential factor on the desorption activation energy; T_Θ is the isokinetic point. (d) Ratio of the desorption rate constant at a fixed potential V^*_{WR} over the desorption rate constant at $V^*_{WR} = 0.06$ V, ρ_d, as a function $1/T$ computed from the low coverage data and Eq. [9] (straight lines) and obtained from the high coverage data of Fig. 13 (filled circles).

defined positive, according to the standard electrochemical convention. When it proceeds to the left the current is defined negative. The remaining part of the current, i.e. that not corresponding to peaks (Figs. 16a and 16b), is due to the charging of the metal–solid electrolyte interface. In fact the double-layer capacitance, C_d, of that interface can be computed from $\delta I = 2\upsilon C_d$, where δI is the "thickness" of the voltammogram and υ is the scan rate (45). The large anodic peak to the right is due to the formation of adsorbed oxygen and the oxygen evolution in the gas phase. Both Figs. 16a and 16b show clearly the reduction ($I < 0$) of the two types of adsorbed oxygen, i.e. normally chemisorbed and ionic at

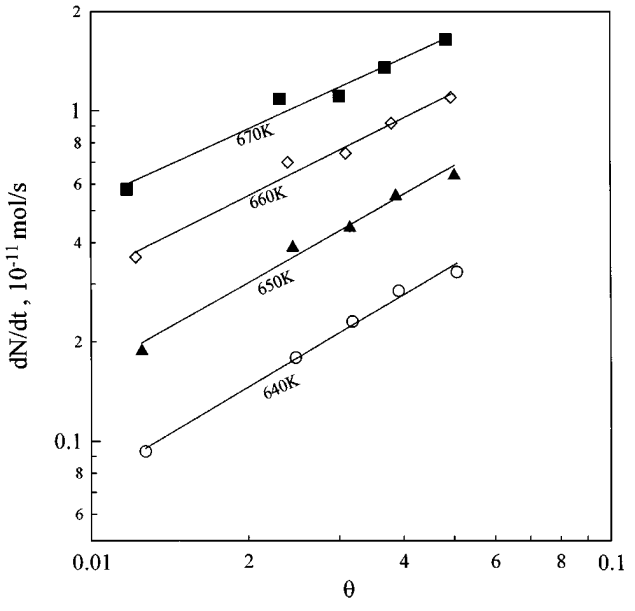

FIG. 15. Desorption rate isotherms obtained from the TPD spectra of Fig. 13 indicating a near first-order desorption rate.

high and low potentials, respectively, in agreement with the exploratory investigation of Yi *et al.* (42). In the presence of gaseous oxygen and short holding times there is only one peak with the second one corresponding to strongly bonded ionic oxygen developing at longer holding times. It is remarkable that, in both cases, the cyclic voltammograms reveal exactly the same feature about the state of adsorbed oxygen as the thermal desorption spectra do. In fact, for long holding times the presence of several states of ionic oxygen is revealed in agreement with the TPD spectra for comparable long current application times during adsorption (Figs. 5a and 7a).

CONCLUSIONS

The present work shows that solid state electrochemistry can be used to affect significantly the binding strength of oxygen on Pt and to create new adsorption states. These results provide a conclusive and rigorous explanation for the physicochemical origin of the effect of nonfaradaic electrochemical modification of catalytic activity (NEMCA) when using O^{2-} conducting solid electrolytes, such as Y_2O_3-doped ZrO_2. The thermal desorption and cyclic voltammetric data are in good agreement with the theory developed previously to explain NEMCA (4) and with the more recent work function (2, 22), XPS (18), and SERS (20) results.

The main conclusions are the following:

1. Electrochemical O^{2-} pumping to Pt catalyst films in the presence of preadsorbed oxygen creates strongly bonded "backspillover" anionic oxygen ($T_p \approx 723$ to 773 K), with a concomitant pronounced lowering of the T_p of the more weakly bound preadsorbed atomic oxygen (up to 50 K, i.e. from 743 to 693 K). The two oxygen species coexist on the surface.

2. The ionic "backspillover" oxygen species does not form via adsorption from the gas phase.

3. At 673 K the ionic backspillover species desorbs at a rate at least seven times slower than that of normally

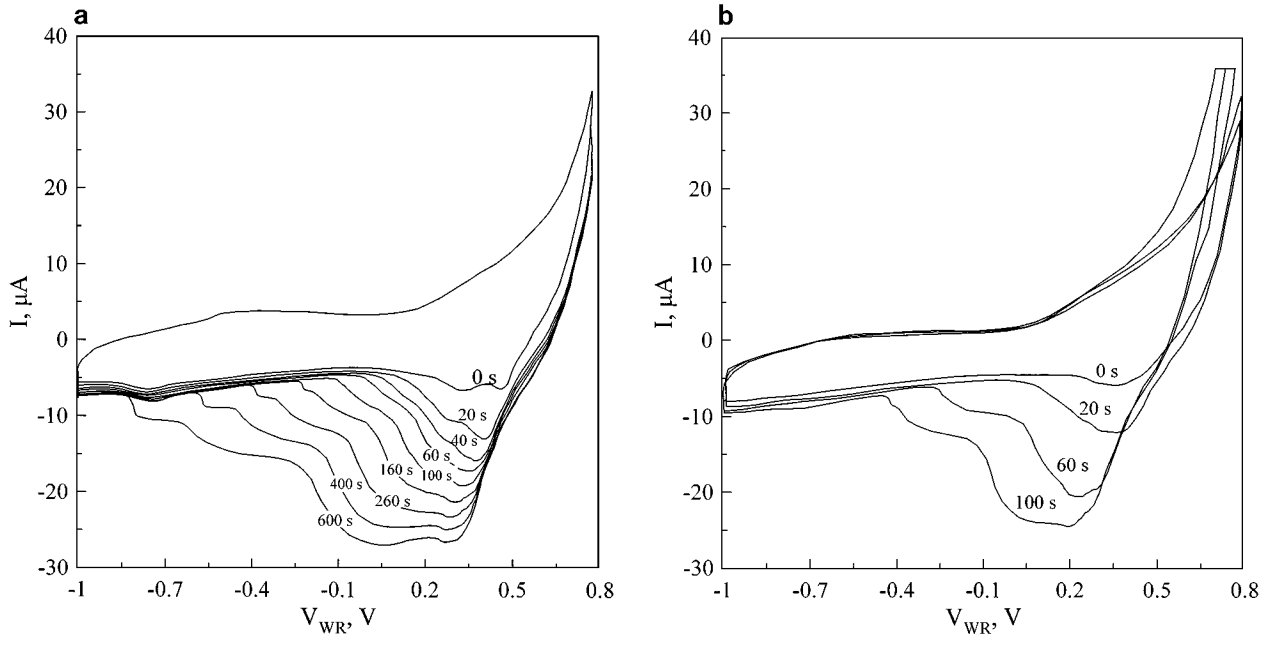

FIG. 16. (a) Cyclic voltammograms of the Pt-film at 673 K and various holding times under UHV. Holding potential: 0.8 *V*; scan rate: 50 mV/s. (b) Cyclic voltammograms of the Pt-film at 673 K and various holding times under $P_{O_2} = 4 \times 10^{-6}$ Torr. Holding potential: 0.8 *V*; scan rate: 50 mV/s.

chemisorbed oxygen. Consequently the reactivity of the two adsorbed oxygen species for catalytic oxidation reactions must also differ significantly and thus the more strongly bonded electrochemically supplied ionic species can act as a sacrificial promoter for catalytic reactions, where the weakly bonded atomic species participates. Since the enhancement factor of faradaic efficiency, Λ, expresses the ratio of catalytic reaction of normally chemisorbed oxygen to that of ionic oxygen (4), the above observation explains directly the high faradaic efficiency, values ($\Lambda \gg 1$) measured in previous NEMCA studies (4).

4. Above 800 K the coverage of ionic oxygen vanishes and, thus, the faradaic efficiency Λ approaches unity, in agreement with experiment (4) (Fig. 11).

5. The pronounced decrease in T_p with increasing potential (from 743 to 693 K), which implies, in view of Fig. 14, a decrease in the binding strength of adsorbed oxygen from 2.14 to 1.42 eV (49 to 33 kcal/mol) causes a pronounced increase in the oxygen desorption rate at any fixed temperature (Fig. 14d). This increase is of the order of 100 at the highest applied potentials (Fig. 14d) which is near the maximum ρ values found in NEMCA studies of catalytic oxidations on Pt.

ACKNOWLEDGMENTS

We thank the PENED Programme of the Hellenic Secretariat of Research and Technology and EPRI (Contract WO 8060-25) for partial financial support and our reviewers for some very thoughtful suggestions.

REFERENCES

1. Vayenas, C. G., Bebelis, S., and Neophytides, S., *J. Phys. Chem*. **92**, 5083 (1988).
2. Vayenas, C. G., Bebelis, S., and Ladas, S., *Nature (London)* **343**, 625 (1990).
3. Vayenas, C. G., Bebelis, S., Yentekakis, I. V., and Lintz, H.-G., *Catal. Today* **11**, 303 (1992).
4. Vayenas, C. G., Jaksic, M. M., Bebelis, S., and Neophytides, S., *in* "Modern Aspects of Electrochemistry" (J. O'M. Bockris, B. E. Conway, and R. E. White, Eds.), Vol. 29, p. 57. Plenum, New York, 1996.
5. Politova, T. I., Sobyanin, V. A., and Belyaev, V. D., *React. Kinet. Catal. Lett.* **41**, 321 (1990).
6. Basini, L., Cavalca, C. A., and Haller, G. L., *J. Phys. Chem*. **88**, 10853 (1994).
7. Harkness, I., and Lambert, R. M., *J. Catal.* **152**, 211 (1995).
8. Chiang, P. C., Eng, D., and Stoukides, M., *J. Catal*. **139**, 683 (1993).
9. Varkaraki, E., Nicole, J., Plattner, E., Comninellis, Ch., and Vayenas, C. G., *J. Appl. Electrochem*. **25**, 978 (1995).
10. Cavalca, C., and Haller, G. L., *J. Catal.*, in press.
11. Palermo, A., Tikhov, M. S., Filkin, N. C., Lambert, R. M., Yentekakis, I. V., and Vayenas, C. G., *Stud. Surf. Sci. Catal.* **101**, 513 (1996).
12. Cavalca, C., Larsen, G., Vayenas, C. G., and Haller, G. L., *J. Phys. Chem*. **97**, 6115 (1993).
13. Pliangos, C., Yentekakis, I. V., Ladas, S., and Vayenas, C. G., *J. Catal.* **159**, 189 (1996).
14. Neophytides, S. G., Tsiplakides, D., Stonehart, P., Jaksic, M. M., and Vayenas, C. G., *Nature (London)* **370**, 45 (1994).
15. Grzybowska-Swierkosz, B., and Haber, J., *in* "Annual Reports on the Progress of Chemistry," Vol. 91, p. 395. The Royal Society of Chemistry, Cambridge, 1994.
16. Pritchard, J., *Nature (London)* **343**, 592 (1990).
17. Bockris, J. O'M., and Minevski, Z. S., *Electrochim. Acta* **39**, 1471 (1994).
18. Ladas, S., Kennou, S., Bebelis, S., and Vayenas, C. G., *J. Phys. Chem*. **97**, 8845 (1993).
19. Zipprich, W., Wiemhöfer, H.-D., Vohrer, U., and Göpel, W., *Ber. Bunsengesel. Phys. Chem*. **99**, 1406 (1995).
20. Kondarides, D. I., Papatheodorou, G. N., Vayenas, C. G., and Verykios, X. E., *Ber. Bunsenges, Phys. Chem*. **97**, 709 (1993).
21. Makri, M., Vayenas, C. G., Bebelis, S., Besocke, K. H., and Cavalca, C., *Surf. Sci.* **369**, 351 (1996).
22. Ladas, S., Bebelis, S., and Vayenas, C. G., *Surf. Sci.* **251/252**, 1062 (1991).
23. Neophytides, S., and Vayenas, C. G., *J. Phys. Chem*. **99**, 17063 (1995).
24. Nicole, J., Tsiplakides, D., Wodiunig, S., and Comninellis, Ch., *J. Electrochem. Soc.* **L312**, 144 (1997).
25. Falconer, J. L., and Madix, R. J., *Surf. Sci.* **48**, 393 (1975).
26. Barteau, M. A., Ko, E. I., and Madix, R. J., *Surf. Sci.* **102**, 99 (1981).
27. Winkler, A., Guo, X., Siddiqui, H. R., Hagans, P. L., and Yates, J. T., *Surf. Sci.* **201**, 419 (1988).
28. Norton, P. R., *Surf. Sci.* **47**, 98 (1975).
29. Derry, G. N., and Ross, P. N., *J. Chem. Phys.* **82**, 2772 (1985).
30. Besocke, K., Krahl-Urban, B., and Wagner, H., *Surf. Sci.* **68**, 39 (1977).
31. Steininger, H., Lehwald, S., and Ibach, H., *Surf. Sci.* **123**, 1 (1982).
32. Kneringer, G., and Netzer, F. P., *Surf. Sci.* **49**, 125 (1975).
33. Norton, P. R., Griffiths, K., and Bindner, P. E., *Surf. Sci.* **138**, 125 (1984).
34. Gland, J. L., and Korchak, V. N., *Surf. Sci.* **75**, 733 (1978).
35. Campbell, C. T., Ertl, G., Kuipers, H., and Segner, J., *Surf. Sci.* **107**, 220 (1981).
36. Gland, J. L., *Surf. Sci.* **93**, 487 (1980).
37. Tsiplakides, D., Neophytides, S., and Vayenas, C. G., in preparation.
38. Habenshaden, E., and Kuppers, J., *Surf. Sci.* **138**, L147 (1984).
39. Pacchioni, S., Ilas, F., Neophytides, S., and Vayenas, C. G., *J. Phys. Chem*. **100**, 16653 (1996).
40. Bond, G. C., "Catalysis by Metals," p. 139. Academic Press, London, 1962.
41. Falconer, J. L., and Madix, R. J., *J. Catal.* **48**, 262 (1977).
42. Yi, J., Kaloyannis, A., and Vayenas, C. G., *Electrochim. Acta* **38**, 2533 (1993).